GRAPHENE OXIDE-BASED HYDROGEL IN PHENOL SENSORS

Razan AL-Zghoul[1], Borhan Albiss[2], Nathir A. F. Al-Rawashdeh[1]

[1]Chemistry Department, Jordan University of Science and Technology
P.O. Box 3030, Irbid 22110, Jordan
roalzghoul20@sci.just.edu.jo (R.A.Z.), nathir@just.edu.jo (N.A.F.A.R.)
[2]Nanotechnology Institute, Jordan University of Science and Technology
P.O. Box 3030, Irbid 22110, Jordan, baalbiss@just.edu.jo (B.A.)

Received 06 November 2024
Accepted 25 May 2025
DOI: 10.59957/jctm.v60.i5.2025.9

ABSTRACT

This study aims to develop and evaluate a nanocomposite hydrogel film sensor for accurately detecting phenol in various real samples. A nanocomposite hydrogel film was synthesised using a three-dimensional network structure formed by poly (vinyl alcohol) (PVA) and gum Arabic (GA) as initiators, graphene oxide (GO) as functional monomers, and citric acid (CA) as a cross-linker. The hydrogel's morphological, structural, and elemental properties were characterised through microscopic and spectroscopic techniques. The hydrogel film-based sensor employed phenol as "imprinted molecules" and phosphate buffer as the solvent. The sensor demonstrated high sensitivity and specificity in detecting phenol within the concentration range of 1 to 50 μM, with a low detection limit of 0.01 mM. The interaction between phenol and the GO nanocomposite within the hydrogel film underpins the sensor's performance. The findings highlight the potential of GO-based hydrogels as high-performance materials for sensing applications. This research advances environmental monitoring technologies, facilitating the accurate and specific recognition of toxic phenolic compounds like phenol in industrial and environmental settings.

Keywords: *hydrogel, graphene oxide, phenol, adsorption, sensor.*

INTRODUCTION

Phenolic compounds are natural bioactive molecules found in plant tissue. Phenol and its derivative compounds, which contain a phenol moiety, are extensively used in various industrial applications, including detergents, pharmaceuticals, oil, petroleum refineries, paper plants, plastic plants, dyes, coal, and chemical synthesis [1, 2]. They used for industrial applications due to their anti-inflammatory, antimicrobial, antioxidant, and anti-proliferative properties. Due to its extensive industrial applicability, it is important to improve and sustain its bioavailability to facilitate the range of applicability [3].

Various analytical methods for monitoring phenol levels include gas chromatography with mass spectrometry, high-performance liquid chromatography, solid-phase microextraction, surface plasmon resonance (SPR), UV spectrophotometry, and chemiluminescence [4]. However, these methods are expensive, time-consuming, and require qualified personnel and skilled analysts [5]. Therefore, developing a simple, inexpensive, real-time analytical technique is ideal for detecting and controlling phenols is essential for managing their impact on industrial processes.

To address the challenges phenol sensors' face, it is essential to fabricate them using materials that offer high sensitivity in physiological environments for detecting low phenol limits. Recently, hydrogel-based sensors have been suggested for phenolic compound sensing [6], due to their high sensitivity to physiological environments and their properties as elastic solids with deformability and fluidity [7].

Hydrogel, a soft material with a three-dimensional hydrophilic polymer network structure, was first discovered in the 1960s [8]. The polymer chains in hydrogels are formed through chemical (covalent bonds)

or physical crosslinking (non-covalent interactions). Due to their highly hydrophilic macromolecular networks, hydrogels exhibit properties of elastic solids with deformability and fluidity. They are well-swollen with water, containing 60 - 90 wt. % water without dissolving [9]. Hydrogels find extensive use in chemical and biological applications, including wearable sensors, agriculture, drug delivery systems, food additives, pharmaceuticals, biomedical applications, tissue engineering, regenerative medicine, wound dressing, and biosensors. These broad applications stem from their unique structure, excellent water swelling, high sensitivity to physiological environments, responsiveness, flexibility, stability, and superior softness [9, 10].

In this research, a nanocomposite hydrogel film was prepared with a three-dimensional network structure using PVA and GA as initiators, GO as functional monomers (GO/ PVA/ GA), and CA as a cross-linker. The incorporation of GO enhances the hydrogel's properties by improving its sensitivity to physiological environments, playing a crucial role in phenol detection. GO, a nanoparticle from the graphene family contains abundant oxygen functional groups such as hydroxyl (OH), carboxyl (-COOH), and epoxy (-C-O-C) [11]. The hybridized carbon atoms on GO are a mix of sp^2 and sp^3 configurations. GO's oxygen content ranges from 30-35 % atomic. These oxygen-containing groups allow GO to be stably dispersed in various organic solvents with abundant functional and polar groups on their basal planes and edges, facilitating strong and compact bonding with fibres and electrical activity. This provides the conditions for preparing high-strength, multifunctional composite hydrogels. Moreover, GO enhances the hydrogel's sensitivity to physiological environments, contributing significantly to phenol detection [12].

PVA is a synthetic polymer characterized by its hydrophilic (OH) groups, high crystallinity, non-toxicity, film-forming properties, water solubility, and excellent biocompatibility. Due to its biodegradability, good hygroscopicity, film-forming ability, sensitivity to pH changes, commercial availability, and superior stretchability, PVA has demonstrated favourable results in sensor applications and health monitoring devices. Consequently, PVA hydrogel is frequently chosen as a sensitive material for chemical sensors. When water is adsorbed onto PVA, the conductivity changes, and hydrogen bonding occurs between the OH groups in PVA and water [13].

GA is a dry secretion extracted from the stems and branches of *Acacia sealosa* in Africa. GA is widely used in preparing network hydrogels due to its biocompatibility, biodegradability, non-toxicity, and gelling properties. However, despite these beneficial properties, GA hydrogels have limitations due to their poor mechanical strength, which restricts their applicability in some areas [14]. To address this limitation, a successful strategy involves incorporating filler materials into the hydrogel, using both organic and inorganic sources [15].

This research involves the synthesis of a PVA/ GA/ GO composite hydrogel and the characterization of its properties using atomic force microscopy (AFM), X-ray diffraction (XRD), Fourier-transform infrared (FT - IR) spectroscopy, and swelling studies. The hydrogel was utilized as a sensor for phenol, and its adsorption capacity and optimal conditions for phenol detection was examined. The binding mechanism was predicted through adsorption kinetics and isotherm models. Additionally, the influence of varying the percentage of GO on the hydrogel's performance was investigated. The findings from this study have significant implications for environmental monitoring and the development of efficient and sensitive sensors for phenolic compounds.

EXPERIMENTAL

Chemicals and solutions

The chemicals and solutions used in this study include graphite (powder, extra pure), sodium nitrate ($NaNO_3$), sulphuric acid (H_2SO_4, 96 %), hydrogen peroxide (H_2O_2, 30 %), potassium permanganate ($KMnO_4$), deionized water (H_2O), CA, GA, PVA, phenol, and phosphate buffer solution (pH = 7).

Preparation of graphene oxide

GO was prepared using Hummers' method, wherein the carbon atoms in graphite were oxidized to produce GO [16]. Initially, 120 mL of sulphuric acid (96 %) was mixed with 2.5 g of sodium nitrate and stirred for a few min. Then, 4.5 g of graphite powder was added, and the mixture was cooled in an ice bath at 0°C for 20 min. Subsequently, 15 g of potassium permanganate ($KMnO_4$) was slowly added while maintaining vigorous stirring and the temperature at 0°C. The mixture was then heated

to 40°C for 2 h with continuous stirring. After this, 250 mL of deionized water was added slowly, keeping the temperature below 50°C. Next, 120 mL of hydrogen peroxide (H_2O_2, 30 %) was slowly added. The mixture was filtered using centrifugation at 7000 rpm, washed with 10 % HCl 3 - 4 times, followed by deionized water 3 - 4 times, resulting in a dark brown paste of GO. Finally, the GO paste was dried in a vacuum oven at 50°C.

Synthesis of PVA/GA/GO based hydrogel

Hydrogels were synthesized by dissolving 1.5 g of PVA in 20 mL of deionized (DI) water and stirring continuously at 90°C for 2 h to form a homogeneous solution. A GA solution was prepared by dissolving 0.5 g of GA in 4 mL of DI water at room temperature and then adding it to the PVA solution along with 0.2 g of citric acid. GO was then added in varying amounts (25 mg, 50 mg, 100 mg, and 150 mg). The resulting viscous liquid was frozen at -15°C for 8 h and then thawed at 25°C for 12 h.

Methods of characterization

The composite hydrogel was characterised using an X-ray diffractometer (XRD-6000 Shimadzu) with Cu Kα radiation (wavelength λ = 0.154 nm) to analyse its crystalline structure and material arrangement. Atomic force microscopy (AIST-NT SmartSPM 1000) was used to investigate the surface morphology and topography. Fourier-transform infrared (FT-IR) spectroscopy (Bruker ALPHA FT - IR spectrometer) identified the chemical bonds and functional groups present in the hydrogel. Swelling studies, which indicate the hydrogel's capacity to absorb and retain water or other fluids, were conducted by submerging the hydrogels in a phosphate-buffered saline (pH = 7). The swelling ratio was calculated using Eq. (1):

$$\text{Swelling ratio} = \frac{(W_s - W_d)}{W_d} 100 \quad (1)$$

where W_s and W_d are the weights of the swollen and dry samples, respectively. The weight of the hydrogel was recorded hourly for the first 5 h, and finally at 24 and 48 h.

Adsorption experimental

The adsorption performance of the hydrogel and its ability to detect phenolic compounds were evaluated at room temperature using a UV-VIS spectrophotometer. The hydrogel (0.1 g) was placed in a 100 mL phosphate buffer solution with phenol. Samples were taken at 15 min intervals to analyse phenol concentration variations. The concentration of phenol was determined by monitoring the maximum absorption peak at 269 nm (λ_{max} for phenol) using a UV-2500PC Shimadzu UV-vis spectrophotometer. A calibration curve was established using phenol solutions (5, 10, 15, 20, and 25 µM; R_2 = 0.9993) to identify the concentration of phenol in unknown samples.

The total percentage of removal efficiency was evaluated using Eq. (2), and the adsorption capacity, Q_e, mg g^{-1}, was calculated using Eq. (3).

$$\text{Re}\,\% = \frac{(C - C_e)}{C} 100\,\% \quad (2)$$

$$Qe = \frac{(C - C_e)V}{m} \quad (3)$$

where C represents the initial concentration of the phenol in phosphate buffer solution, while C_t is the concentration of phenol after adsorption. V (mL) represents the solution volume, and m (g) represents the mass of GO-hydrogel.

RESULTS AND DISCUSSION

FT - IR analysis

The FT - IR spectrum of GO was recorded at room temperature in the wavenumber range of 650 to 4000 cm^{-1}, as shown in Fig. 1a. The absorption peak at 1029 cm^{-1} corresponds to alkoxy (C-O) bending, 1222 cm^{-1} is ascribed to epoxy (C-O), 1619 cm^{-1} refers to remaining sp^2 (C=C) bonds, and 1707 cm^{-1} is attributed to the carbonyl (C=O) group. The absorption peaks between 3050 cm^{-1} and 3800 cm^{-1} are due to the stretching of the hydroxyl (O-H) bonds. These results confirm the formation of GO, aligning with other studies, which demonstrate the chemical inertness of bulk graphite [16].

The spectra for PVA and GA are presented in Fig. 1a. PVA exhibits strong vibrational peaks at 1099 cm^{-1} (C-O stretching), 1419 cm^{-1} (CH_3 bending and C-H bending), and 1713 cm^{-1} [carbonyl (C=O) stretching]. The bands between 3550 and 3200 cm^{-1} are attributed to (O-H) bonds from intermolecular and intramolecular hydrogen bonds. The vibrational band between 2840 and 3000 cm^{-1} corresponds to the stretching of C-H

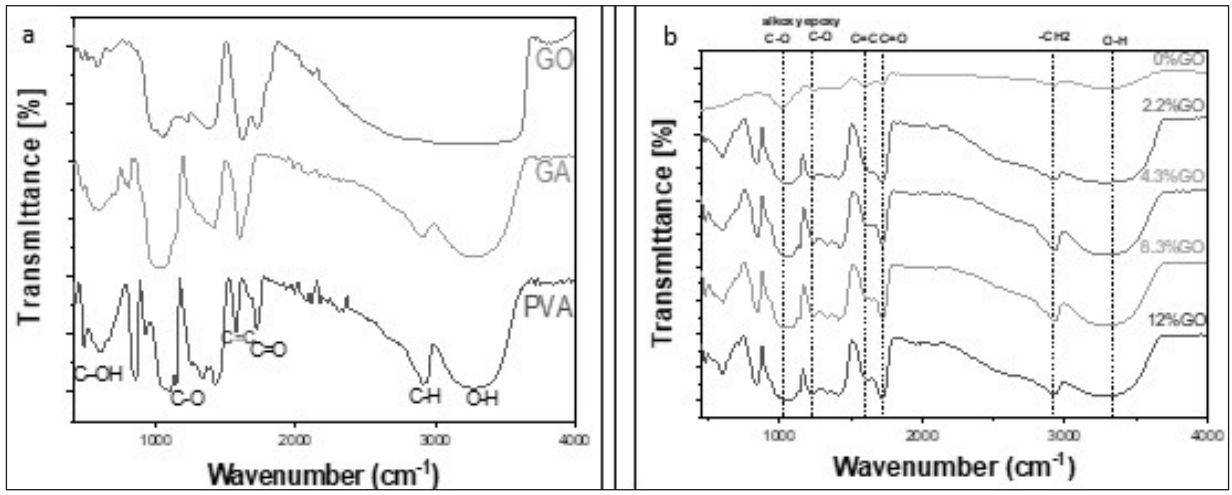

Fig. 1. (a) Fourier transform infrared (FT-IR) spectra of GO, PVA and GA; (b) FT-IR spectra of hydrogels at different concentrations of GO.

from alkyl groups. GA displays characteristic bands at 3256 cm^{-1}, representing (O-H). The band at 2928 cm^{-1} is due to aliphatic groups (-CH_2, -CH_3), indicating the presence of sugars such as arabinose, galactose, and rhamnose [17]. The bands observed between 1225, and 1410 cm^{-1} are from polysaccharides and galactoproteins, referring to CH_3 bend, (C=C) stretch, ketone (C-C) stretch, carboxylic acid (C-O) stretch, and amine (C-N) stretch. The absorption peak at 1017 cm^{-1}, due to the (C-O-C) and (C-OH) vibrations, indicates the presence of pyranose units in the structure [18].

The effect of different concentrations of GO on the hydrogel was studied using FT - IR, as shown in Fig. 1b. The changes in the intensity and shape of FT - IR peaks in the hydrogel spectra with varying concentrations of GO provide insights into the interaction between GO and the hydrogel. The results indicate that the hydroxyl peak has shifted, and its intensity has changed, suggesting the formation of hydrogen bonding between GO sheets and PVA chains. This is evidenced by the interaction of the carbonyl group in GO with the hydroxyl group of PVA. Additionally, the stretching vibration of C=O shifts and appears with higher intensity, indicating the establishment of a hydrogen bond between C=O and OH. Furthermore, the disappearance of the (CO-H) band in PVA in the FT-IR spectra of the hydrogel suggests interaction between PVA and GO.

XRD analysis

The XRD pattern for GO, PVA, and GA is depicted in Fig. 2a. For GO, peaks were observed at 2θ values of 10.64° and a small peak at 21.2°, with interlayer spacing of 4.172 Å and 2.13 Å, respectively. These results are consistent with previous findings, where graphite exhibited strong peaks at 2θ = 26.5° and a slight peak at 2θ = 54.5°, corresponding to d-spacing of 3.5 Å and 1.9 Å, confirming successful GO synthesis [19]. The XRD pattern of PVA reveals peaks at 2θ values of 19.48° and 40.84°, indicating interlayer spacing of 2.31 Å and 1.18 Å, respectively. Meanwhile, GA shows a broad peak at 2θ = 18.47° with an interlayer spacing of 2.43 Å.

Fig. 2b. illustrates the XRD patterns for the hydrogel with varying concentrations of GO (0 %, 2.2 %, 4.3 %, 8.3 %, and 12 %). The diffraction peaks shift to 2θ values of 20.4°, 20.08°, 19.50°, 19.42°, and 19.38°, corresponding to interlayer spacing of 2.21 Å, 2.24 Å, 2.31 Å, 2.32 Å, and 2.32 Å, respectively. These peaks align well with the typical diffraction peaks of PVA at 2θ = 19.48°, indicating successful incorporation and dispersion of GO in the PVA and GA matrix. The observed shift in peaks suggests an increase in crystallinity after hydrogel formation, indicating a more uniform crystal structure. This improvement in crystallinity can be attributed to the dispersion of GO sheets in PVA and GA, facilitated by hydrogen bonding between oxygen-containing groups in GO and hydroxyl groups in PVA and GA. The intensity and width of the hydrogel peaks increase with higher GO contents, indicating enhanced crystallinity with increased GO concentration. In summary, the presence of oxygen-

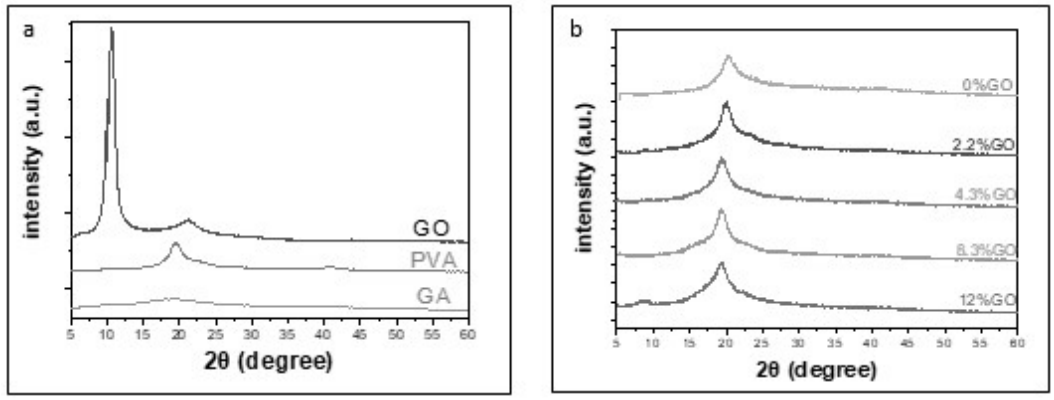

Fig 2. (a) X-ray diffraction (XRD) patterns of GO, PVA and GA; (b) XRD patterns for the prepared hydrogels with different concentrations of GO.

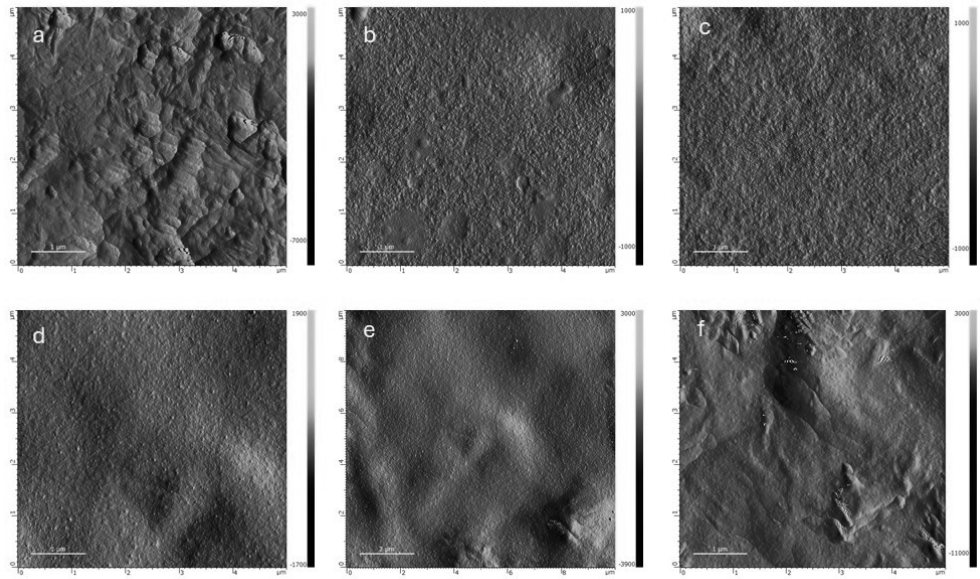

Fig. 3. AFM image for (a) GO; (b) 0 % GO- hydrogel; (c) 2.2 % GO- hydrogel; (d) 4.3 % GO- hydrogel; (e) 8.3 % GO-hydrogel; (f) 12 % GO- hydrogel.

functional groups in GO significantly influences the crystallinity of the hydrogel. Higher concentrations of GO, particularly at 12 %, exhibit the most pronounced crystallinity, evidenced by the sharpest and highest peaks in the hydrogel pattern.

AFM

The morphology of the hydrogel was analysed using AFM. Fig. 3a illustrates AFM images of GO sheets, showing diverse and irregular shapes indicative of disrupted interlayer order due to the presence of oxygen-containing functional groups. This observation confirms the successful oxidation of graphite to produce GO [20]. Fig. 3b presents AFM images of (GO/PVA/GA) hydrogels with varying concentrations of GO. Higher concentrations of GO lead to more uniform dispersion or aggregation of GO Nano sheets, as evidenced by the AFM images. The hydrogel surfaces appear smooth and homogeneous, indicating minimal visible pores within the structure. This suggests effective interaction and infiltration of PVA and GA into the GO sheets, filling the gaps between the sheets. The good infiltration of

PVA and GA into the GO sheets enhances the adhesion between PVA, GA, and GO, thereby contributing to improved mechanical properties of the hydrogel. In summary, AFM analysis confirms the uniform dispersion or aggregation of GO Nano sheets within the hydrogel matrix, highlighting the effective integration of PVA, GA, and GO components.

Swelling performance of hydrogel

The swelling behaviour of (GO/ GA/ PVA) hydrogels, indicative of their high hydrophilic nature, was thoroughly investigated in this study. Fig. 4a illustrates the swelling kinetics of the hydrogel samples over time, showing a rapid increase in swelling rate from 0 to 48 h. Notably, the hydrogel without GO exhibits the fastest swelling rate, whereas the hydrogel containing 12 % GO demonstrates the slowest swelling rate.

Fig. 4b. further details the swelling ratios of (GO/ GA/ PVA) hydrogels containing varying concentrations of GO after 48 h. The swelling ratios for hydrogels with 0 %, 2.2 %, 4.3 %, 8.3 %, and 12 % GO are recorded as 708.3 %, 352.2 %, 288 %, 233.3 %, and 203.6 %, respectively. These results underscore the significant influence of GO content on the swelling properties of the hydrogels. The interaction between GO sheets and the polymeric network of the hydrogel, facilitated by both covalent and non-covalent bonding, plays a crucial role in modulating the hydrogel's structure and swelling behaviour.

The observed differences in swelling ratios highlight the intermolecular interactions within the hydrogel network, wherein the incorporation of GO restricts swelling due to enhanced structural integrity. Additionally, hydrogen bonding between GO sheets and the hydrogel further enhances mechanical properties. The unique structure and high surface area of GO also contribute to minimizing interactions with phosphate buffer within the polymeric hydrogel network, affecting the overall swelling behaviour [21].

The adsorption efficiency of the GO-hydrogel for phenol removal

The evaluation of phenol detection was conducted under specific conditions, focusing on the adsorption capacity of GO within the hydrogel. This study examined the adsorption of phenol by hydrogels containing varying concentrations of GO (0, 25, 50, 100, and 150 mg) to assess their efficacy as phenol sensors. Among the samples, the hydrogel with 8.3 % wt. GO exhibited the highest phenol removal efficiency at 54 %. This was followed by hydrogels with 12 % wt., 4.3 % wt., 2.2 % wt., and 0 % wt. GO, which showed removal efficiencies of 52 %, 54 %, 46.5 %, 44.5 %, and 24.2 %, respectively, as depicted in Fig. 5.

Fig. 6 shows the UV-Vis absorbance spectra of hydrogels containing varying concentrations of GO, ranging from 0 % to 12 %. Each sub-figure displays absorbance as a function of wavelength (nm), revealing characteristic peaks around 260 nm. As the GO content

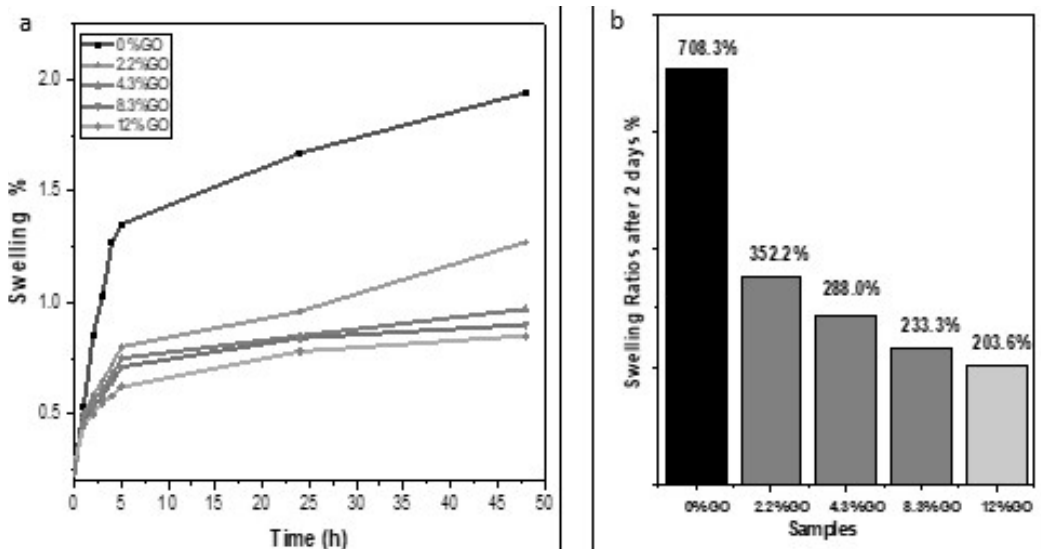

Fig. 4. (a) Swelling behaviour of hydrogel samples at separate times; (b) Compare swelling ratios between samples.

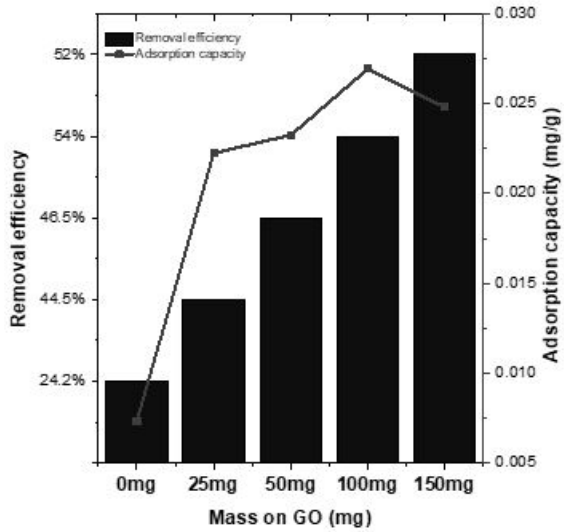

Fig. 5. The removal efficiency % and adsorption capacity of phenol.

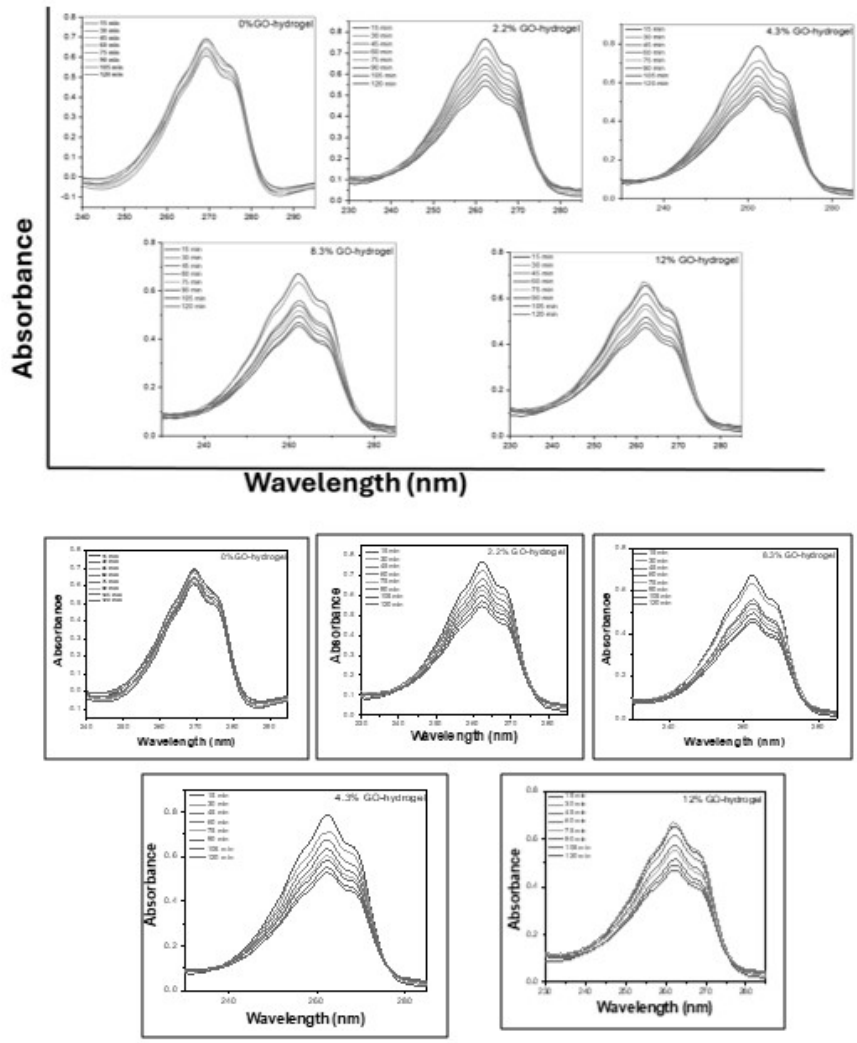

Fig. 6. UV-Vis spectra for (a) 0 % GO- hydrogel; (b) 2.2 % GO- hydrogel; (c) 4.3 % GO- hydrogel; (d) 8.3 % GO- hydrogel; (e) 12 % GO- hydrogel.

increases, a gradual change in absorbance intensity is observed, indicating interactions between GO and the hydrogel matrix. The consistent peak positions across all samples suggest similar electronic transitions, while variations in intensity reflect the influence of GO concentration on the optical properties of the hydrogels. The spectral changes observed in Fig. 6. result from the interaction between phenol and GO within the hydrogel matrix. Several factors contribute to this enhanced adsorption efficiency:

- **Strong interaction forces**: Phenol molecules exhibit strong interaction forces with GO, such as Van der Waals forces and electrostatic interactions. These forces facilitate the attachment of phenol molecules to the GO surface, resulting in higher adsorption.
- **Accessible active sites**: GO has a high surface area and is rich in oxygen-containing functional groups, such as carboxyl and hydroxyl groups. These functional groups provide active sites for phenol molecules to interact and adsorb onto the GO surface.
- **Available surface sites on hydrogel**: The hydrogel surface also provides sites for phenol adsorption. The presence of GO increases the surface area and available adsorption sites, thereby enhancing adsorption efficiency.

Combining the hydrogel with the unique properties of GO results in a highly effective system for phenol adsorption. The interaction between phenol molecules and GO within the hydrogel likely involves a combination of chemical and physical interactions, making this composite an efficient and viable method for phenol removal from various environmental and industrial sources. Understanding how GO concentration affects phenol adsorption efficiency in the hydrogel can aid in optimizing the material for practical applications and environmental remediation purposes.

Adsorption kinetics

Adsorption kinetics research is crucial for determining the efficiency of an adsorbent and understanding the mechanism of adsorption. The adsorption kinetics results were modelled using the pseudo-first-order Eq. (4), pseudo-second-order Eq. (5), and intra-particle diffusion model Eq. (6).

$$\ln(Q_e - Q_t) = \ln Q_e - K_1 t \quad (4)$$

$$\frac{t}{Q_t} = \frac{1}{K_2 Q_2} + \frac{1}{Q_e} t \quad (5)$$

$$Q_t = K_{id}\, t^{0.5} + c \quad (6)$$

where t (h) is time, Q_e (mg g^{-1}) is the adsorbed amount at equilibrium, Q_t (mg g^{-1}) is the adsorbed amount at different times, K_1 (min^{-1}) is the rate constant of the pseudo-first-order model, K_2 (g mg^{-1} min^{-1}) is the rate constant of the pseudo-second-order model, K_{id} (mg g^{-1} $min^{-1/2}$) is the intra-particle diffusion rate constant, and c is a constant.

Fig. 5. illustrates the results of fitting several models to the adsorption kinetics of phenol onto GO in hydrogels with different GO concentrations (25, 50, 100, and 150 mg). The parameters for adsorption kinetics are presented in Table 1. Across all stirring rate models, it is evident that the phenol adsorption rate is rapid within the first 30 min.

Fig. 7a. depicts the curve fit of the pseudo-first-order model. The results indicate that this model is inapplicable for the system, as the experimental data deviate from linearity, and the rate constant K^1 is low, as

Table 1. Kinetic model parameters for adsorption of phenol onto.

Kinetic models	Parameter	2.2 % GO	4.3 % GO	8.3 % GO	12 % GO
Pseudo-first-order	k_1 (min^{-1})	0.03	0.034	0.037	0.040
	Q_e (mg g^{-1})	0.10	0.061	0.028	0.022
	R^2	0.84	0.88	0.88	0.81
Pseudo-second-order	K_2 (min^{-1})	0.36	0.54	1.9	3.18
	Q_e (mg g^{-1})	0.104	0.06	0.03	0.019
	R^2	0.98	0.98	0.99	0.99
Intra-particle diffusion	K_{id} (mg g^{-1} $min^{0.5}$)	0.40	0.44	0.49	0.44
	C (mg g^{-1})	0.45	0.32	0.87	0.9
	R^2	0.96	0.98	0.90	0.87

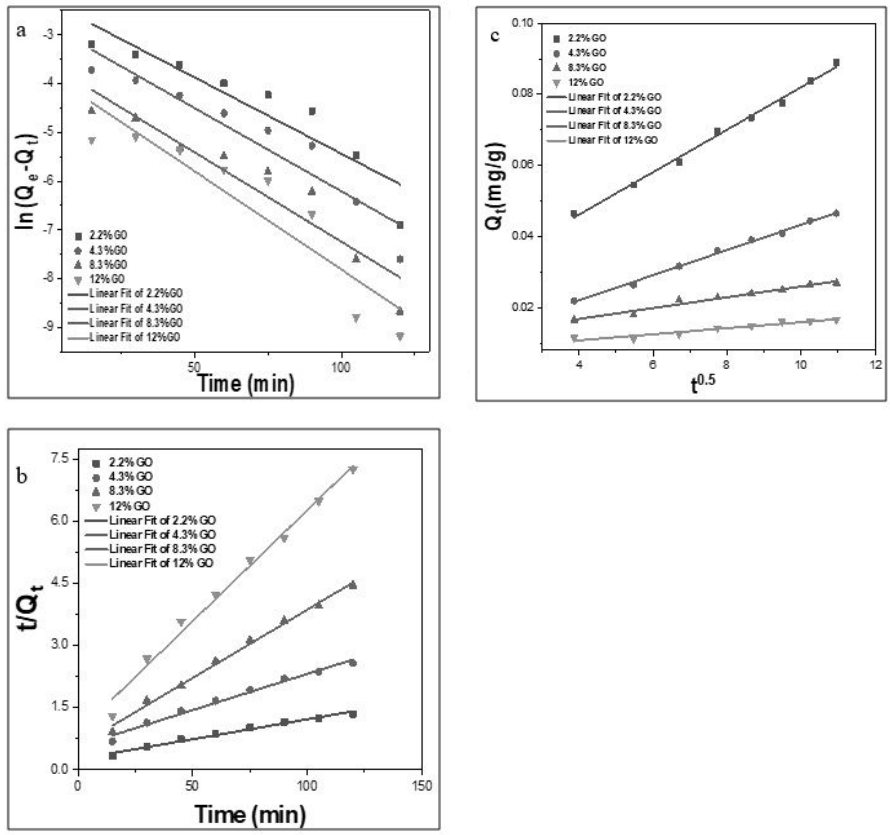

Fig. 7. (a) Adsorption kinetics curve fitting for pseudo-first-order model; (b) Adsorption kinetics curve fitting for pseudo-second order model; (c) Adsorption kinetics curve fitting for Intra-particle diffusion model.

shown in Table 1. Conversely, Fig. 7b. shows the curve fit of the pseudo-second-order model. The plot forms a straight line, indicating that the linearized form of the pseudo-second-order model adequately describes the adsorption process. A straight-line relationship suggests better linearity, making the model a good representation of the adsorption kinetics [22].

The coefficient of determination (R^2) is used to compare the pseudo-first and pseudo-second-order kinetic models. Higher R^2 values indicate a better explanation of the system's adsorption kinetics. As shown in Table 1, the pseudo-second-order kinetic model has a substantially higher R^2 value than the pseudo-first-order model, indicating it better describes the experimental data.

To simulate system data and better understand the factors influencing adsorption kinetics, the intra-particle diffusion model was employed. If intra-particle diffusion is the rate-limiting step, the plot of Q_t vs. t 0.5 should be linear, and the data should pass through the origin (intercept = 0). The results in Fig. 7c. and Table 1 show that the plot of Q_t vs. t 0.5 yields four straight lines but does not pass through the origin, indicating that intra-particle diffusion is influenced by other kinetic effects.

In summary, the pseudo-second-order kinetics model aligns well with this system, confirming that surface adsorption involves physicochemical interactions between phenol and GO, resulting in phenol removal from the solution. Additionally, the intra-particle diffusion model suggests that adsorption is influenced by intra-particle diffusion along with other kinetic effects.

Table 1 presents the kinetic model parameters for the adsorption of phenol onto hydrogels with varying GO concentrations. The pseudo-first-order model shows that the rate constant k^1 ranges from 0.03 to 0.040 min^{-1}, with equilibrium adsorption capacity (Q_e) between 0.022 and 0.10 mg g^{-1}, and R^2 values ranging from 0.81 to 0.88, indicating a poor fit. The pseudo-second-order model demonstrates a better fit with R^2 values of 0.98 to 0.99, rate constants (K^2) from 0.36 to 3.18 min^{-1},

and Q_e values decreasing from 0.104 to 0.019 mg g^{-1} as GO concentration increases. The intra-particle diffusion model indicates K_{id} values between 0.40 and 0.49 mg g^{-1} $min^{-0.5}$, C values from 0.32 to 0.9 mg g^{-1}, and R^2 values from 0.87 to 0.98, suggesting that intra-particle diffusion influences adsorption alongside other kinetic effects. Overall, the pseudo-second-order model best describes the adsorption kinetics for this system.

Adsorption isotherm

An adsorption isotherm is a fundamental relationship describing how solute molecules in phenol adhere to GO in hydrogel at a given temperature and pressure, forming either a monolayer or multiple layers of adsorbate molecules on the surface. To further investigate the adsorption mechanism of phenol by GO in hydrogel, the isothermal adsorption of phenol was analysed using the Langmuir Eq. (7) and Freundlich models Eq. (8) [23].

$$Q_e = \frac{Q_m K_1 C_e}{1 + K_1 C_e} \quad (7)$$

$$Q_e = K_f C e^{\frac{1}{n_f}} \quad (8)$$

where Q_e (mg g^{-1}) is the adsorbed amount at equilibrium time, Q_m (mg g^{-1}) is the theoretical saturated adsorption amount, C_e (mg L^{-1}) is the equilibrium concentration of phenol, K_l (L mg^{-1}) is the Langmuir constant, K_f (mg g^{-1}) is the Freundlich constant, and n_f is a heterogeneous coefficient (dimensionless).

Fig. 8 shows the data from the isothermal adsorption of phenol analysed using the Langmuir model (Fig. 8a) and the Freundlich model (Fig. 8b). The parameters calculated from these two isotherms are presented in Table 2. The models' applicability was evaluated based on the residual sum of squares (RSS) and coefficient of determination (R^2) values to determine the best-fitting equilibrium model. A better fit is indicated by lower RSS values and higher R^2 values. By comparing these values, the Langmuir model exhibited lower RSS values than the Freundlich model, and the R^2 values in the Freundlich adsorption isotherm were very high and close to those in the Langmuir model.

The Langmuir isotherm can be expressed in terms of a dimensionless factor called the separation factor (R_L), defined by Eq. (9):

$$R_L = \frac{1}{1 + K_l C_0} \quad (9)$$

The R_L value indicates the type of isotherm: irreversible adsorption ($R_L = 0$), favourable adsorption ($0 < R_L < 1$), linear adsorption ($R_L = 1$), and unfavourable adsorption ($R_L > 1$) [24]. In this study, the R_L values were smaller than 1, confirming the favourability of adsorption and the applicability of the Langmuir isotherm.

In the Freundlich isotherm, the n_f value indicates the suitability of the adsorption process. The process is considered favourable when $1 < n_f < 10$, implying stronger interaction between the adsorbent and the adsorbate. An n_f value of 1 indicates linear and favourable adsorption, while n_f less than 1 suggests that the interaction between the solute and the adsorbent

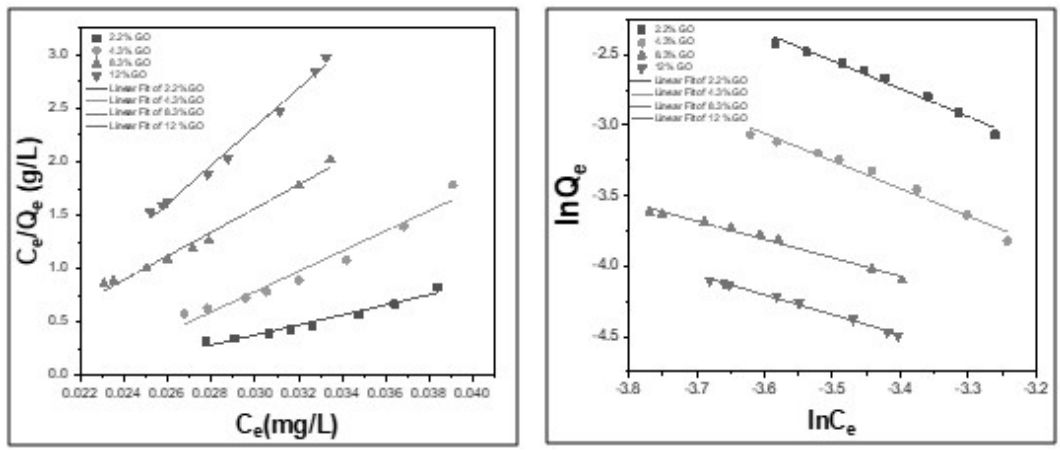

Fig. 8. (a) Fitted Langmuir mode adsorption curve; (b) Fitted Freundlich model adsorption curve.

is unfavourable, indicating lower efficiency at higher solute concentrations. In this study, the n_f values were less than 1 for all samples, indicating unfavourable interaction in the Freundlich isotherm and increased non-linearity and decreased adsorption efficiency as solute concentration increases. The results demonstrated that adsorption follows the Langmuir isotherm, indicating monolayer adsorption and homogeneous adsorption on the surface [25].

Table 2 shows that the Langmuir model fits the adsorption of phenol onto GO hydrogel better than the Freundlich model. The maximum adsorption capacity (Q_m) increases with GO concentration, peaking at 3.89 mg/g for 8.3 % GO. The Langmuir constant (K^1) and high R^2 values (0.95 to 0.99) suggest strong adsorption affinity and a good model fit, with low RSS values indicating minimal error. The separation factor (R_L) values, all less than 1, confirm favourable adsorption. In contrast, the Freundlich model shows less favourable adsorption with negative n_f values, higher RSS, and similarly high R^2 values, indicating it is less suitable. Thus, the Langmuir isotherm better describes the adsorption process, indicating monolayer adsorption on a homogeneous surface.

Effect of phenol concentration

After optimizing the GO concentration in the hydrogel, the effect of phenol concentration on sensing performance was assessed by examining different samples with phenol concentrations ranging from 1 to 50 µM. Fig. 9 shows that phenol's removal efficiency decreases with increasing phenol concentration, with the lower limit for visual detection found to be 0.01 µM. The results indicate that higher phenol concentrations reduce the adsorption capacity of the GO. Several factors can explain this decrease in sensor performance with increasing phenol concentration:

- Active sensing sites may saturate more quickly as phenol concentration increases. Initially, there are sufficient unoccupied sites for phenol molecules, but as the concentration rises, these sites become saturated faster, reducing the sensor's response [26].
- Competition among phenol molecules for active sites on the GO surface can occur at higher concentrations, limiting the accessibility of these sites and reducing the sensor's response [27].
- The surface-related phenomenon: As the number of phenol molecules in solution increases relative to the available active adsorption sites on the GO surface, the initial phenol concentration will saturate these sites, thus decreasing removal efficiency [26].
- Thick adsorbed layer formation: Higher phenol concentrations may lead to a thick adsorbed layer on

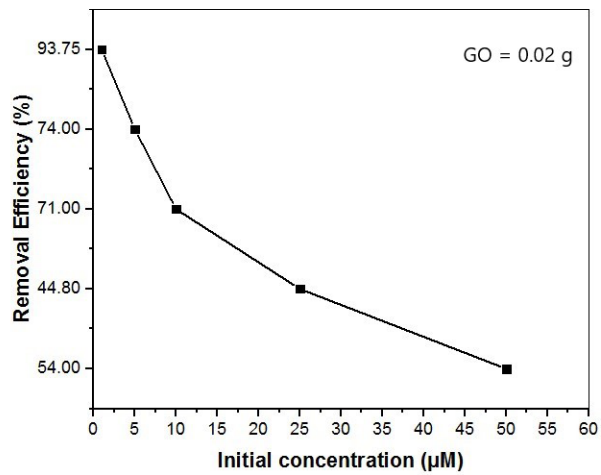

Fig. 9. The effect of initial concentration on the adsorption.

Table 2. Isotherm Model Parameters for Adsorption.

Adsorption isotherms	Parameter	2.2 % GO	4.3 % GO	8.3 % GO	12 % GO
Langmuir model	Q_m, mg g $^{-1}$	2.92	2.75	3.89	3.85
	K_l, L mg^{-1}	646.19	1346.3	3634.6	1119.6
	R^2	0.96	0.95	0.98	0.99
	RSS	2.6×10^{-6}	4.76×10^{-6}	4.6×10^{-7}	2.1×10^{-7}
	R_L	0.03	0.015	0.005	0.018
Freundlich model	K_f, mg g^{-1}	7.79×10^{-5}	4.16×10^{-5}	2×10^{-4}	9.35×10^{-5}
	n_f	-0.506	-0.51	-0.768	-0.71
	R^2	0.98	0.97	0.98	0.99
	RSS	0.0068	0.012	0.003	0.001

the GO surface, hindering phenol molecules' access to active sites and reducing sensor efficacy. utilized interlayer-modified titanium nanotubes to analyse phenol adsorption, finding that the elimination percentage of phenol decreases as the initial concentration increases. Similarly, higher initial phenol concentrations diminish the adsorption capacity of GO [26].

CONCLUSIONS

In conclusion, this study has demonstrated the development and effectiveness of a hydrogel sensor utilizing functionalized GO nanocomposite for phenol detection. The sensor achieved a high phenol adsorption efficiency of 54 %, with a sample containing 8.33 % GO. The adsorption process followed pseudo-second-order kinetics, indicating physicochemical interactions between phenol and GO, and was also influenced by intra-particle diffusion. Isothermal adsorption studies showed that phenol adsorption adhered to the Langmuir isotherm, suggesting monolayer and homogeneous adsorption. The sensor exhibited a responsive range of 1-50 μM for phenol, with a detection limit of 0.01 μM. These findings underscore the sensor's high sensitivity, specificity, and ease of use, making it a promising tool for environmental monitoring and pollutant detection.

Acknowledgments

The financial support from the Deanship of Research/Jordan University of Science and Technology is appreciatively acknowledged.

Authors' contributions: *R.AL-Z. Conducted experiments, data collection, and initial data analysis; B.A. Contributed to data interpretation and provided critical insights in chemical synthesis and analytical characterization; N.A.F.Al-R. Conceptualized and supervised the study, designed the methodology, and drafted and finalized the manuscript. All authors reviewed and approved the final manuscript.*

REFERENCES

1. A. Aisami, M. Usman, A. Siddan, M. Ramlatu, I. James, L. Garba, N. Yasid, M. Shukor, Yield coefficient for the growth of Pseudomonas sp. AQ5-04 at various concentrations of phenol, African Journal of Biotechnology, 19, 2020, 400-407.
2. M. Hosseini Aliabadi, N. Esmaeili, H. Samari Jahromi, An electrochemical composite sensor for phenol detection in waste water, Applied Nanoscience, 10, 2020, 597-609.
3. B.R. Albuquerque, S.A. Heleno, M.B.P. Oliveira, L. Barros, I.C. Ferreira, Phenolic compounds: Current industrial applications, limitations and future challenges, Food & function, 12, 2021, 14-29.
4. A. Pathak, B.D. Gupta, Fiber-optic plasmonic sensor utilizing CTAB-functionalized ZnO nanoparticle-decorated carbon nanotubes on silver films for the detection of catechol in wastewater, ACS Applied Nano Materials, 3, 2020, 2582-2593.
5. I. Delfino, N. Diano, M. Lepore, Advanced Optical Sensing of Phenolic Compounds for Environmental Applications, Sensors, 21, 2021, 7563.
6. L. Zhang, L. Sun, T. Su, T. Chen, L. Hu, F. He, H. Xu, Graphene-based hydrogel with embedded gold nanoparticles as a recyclable catalyst for the degradation of 4-nitrophenol, Colloids and Surfaces A: Physicochemical and Engineering Aspects, 640, 2022, 128410.
7. Y. Chae, L. Kim, D. Kim, R. Cui, J. Lee, Y.-J. An, Deriving hazardous concentrations of phenol in soil ecosystems using a species sensitivity distribution approach, Journal of Hazardous Materials, 399, 2020, 123036.
8. L. Fu, A. Yu, G. Lai, Conductive hydrogel-based electrochemical sensor: A soft platform for capturing analyte, Chemosensors, 9, 2021, 282.
9. S. Bashir, M. Hina, J. Iqbal, A. Rajpar, M. Mujtaba, N. Alghamdi, S. Wageh, K. Ramesh, S. Ramesh, Fundamental concepts of hydrogels: Synthesis, properties, and their applications, Polymers, 12, 2020, 2702.
10. T. Zhu, Y. Ni, G.M. Biesold, Y. Cheng, M. Ge, H. Li, J. Huang, Z. Lin, Y. Lai, Recent advances in conductive hydrogels: classifications, properties, and applications, Chemical Society Reviews, 52, 2023, 473-509.
11. C. Peng, X. Zhang, Chemical functionalization of graphene nanoplatelets with hydroxyl, amino, and carboxylic terminal groups, Chemistry, 3, 2021, 873-888.
12. J. Yi, G. Choe, J. Park, J.Y. Lee, Graphene oxide-

incorporated hydrogels for biomedical applications, Polymer Journal, 52, 2020, 823-837.
13. S. Azadi, S. Peng, S.A. Moshizi, M. Asadnia, J. Xu, I. Park, C.H. Wang, S. Wu, Biocompatible and highly stretchable PVA/AgNWs hydrogel strain sensors for human motion detection, Advanced Materials Technologies, 5, 2020, 2000426.
14. Q. Cao, Z. Shu, T. Zhang, W. Ji, J. Chen, Y. Wei, Highly elastic, sensitive, stretchable, and skin-inspired conductive sodium alginate/polyacrylamide/gallium composite hydrogel with toughness as a flexible strain sensor, Biomacromolecules, 23, 2022, 2603-2613.
15. X. Wang, W. Wei, Z. Guo, X. Liu, J. Liu, T. Bing, Y. Yu, X. Yang, Q. Cai, Organic–inorganic composite hydrogels: compositions, properties, and applications in regenerative medicine, Biomaterials Science, 12, 2024, 1079-1114.
16. X. Chen, Z. Qu, Z. Liu, G. Ren, Mechanism of oxidization of graphite to graphene oxide by the hummers method, ACS omega, 7, 2022, 23503-23510.
17. E. Abba, Z. Shehu, R.M. Haruna, Green synthesis and characterization of CuO@SiO_2 nanocomposite using gum Arabic (Acacia senegalensis)(L) against malaria vectors, Trends in Sciences, 18, 2021, 28.
18. N. Thombare, A. Mahto, D. Singh, A.R. Chowdhury, M.F. Ansari, Comparative FTIR characterization of various natural gums: a criterion for their identification, Journal of Polymers and the Environment, 31, 2023, 3372-3380.
19. S. Nagappan, M. Duraivel, S. Han, M. Yusuf, M. Mahadadalkar, K. Park, A. Dhakshinamoorthy, K. Prabakar, S. Park, C.-S. Ha, Electrocatalytic oxygen reduction reaction of graphene oxide and metal-free graphene in an alkaline medium, Nanomaterials, 13, 2023, 1315.
20. H. Yu, Y. He, G. Xiao, Y. Fan, J. Ma, Y. Gao, R. Hou, X. Yin, Y. Wang, X. Mei, The roles of oxygen-containing functional groups in modulating water purification performance of graphene oxide-based membrane, Chemical Engineering Journal, 389, 2020, 124375.
21. I. Zare, M. Mirshafiei, B. Kheilnezhad, B.F. Far, M. Hassanpour, E. Pishbin, S.S.E. Vaghefi, F. Yazdian, H. Rashedi, A. Hasan, Hydrogel-integrated graphene superstructures for tissue engineering: from periodontal to neural regeneration, Carbon, 2024, 118970.
22. Q. Wang, J. Shao, J. Xu, F. Dong, Y. Xiong, Q. Chen, In-situ formed Cyclodextrin-functionalized graphene oxide/poly (N-isopropylacrylamide) nanocomposite hydrogel as an recovery adsorbent for phenol and microfluidic valve, Journal of Colloid and Interface Science, 607, 2022, 253-268.
23. B. Xie, J. Qin, S. Wang, X. Li, H. Sun, W. Chen, Adsorption of phenol on commercial activated carbons: modelling and interpretation, International Journal of Environmental Research and Public Health, 17, 2020, 789.
24. O.G. Okpara, O.M. Ogbeide, O.C. Ike, K.C. Menechukwu, E.C. Ejike, Optimum isotherm by linear and nonlinear regression methods for lead (II) ions adsorption from aqueous solutions using synthesized coconut shell-activated carbon (SCSAC), Toxin Reviews, 40, 2021, 901-914.
25. S. Kalam, S.A. Abu-Khamsin, M.S. Kamal, S. Patil, Surfactant adsorption isotherms: A review, ACS omega, 6, 2021, 32342-32348.
26. M.A. Al-Ghouti, J. Sayma, N. Munira, D. Mohamed, D.A. Da'na, H. Qiblawey, A. Alkhouzaam, Effective removal of phenol from wastewater using a hybrid process of graphene oxide adsorption and UV-irradiation, Environmental Technology and Innovation, 27, 2022, 102525.
27. L. Ge, S.-P. Li, G. Lisak, Advanced sensing technologies of phenolic compounds for pharmaceutical and biomedical analysis, Journal of pharmaceutical and biomedical analysis, 179, 2020, 112913.